ELSEVIER

Thermochimica Acta 304/305 (1997) 303–316

thermochimica acta

AC calorimetric studies of phase transitions in porous substrates. Superfluid helium and liquid crystals

Daniele Finotello*, Sihai Qian, Germano S. Iannacchione[1]

Department of Physics and Liquid Crystal Institute, Kent State University, Kent, OH 44242, USA

Received 2 August 1996; accepted 14 March 1997

Abstract

In this review, we detail the application of an AC calorimetry technique as it has been employed and optimized for the study of phase transitions, particularly the superfluid-to-normal transition and those undergone by liquid crystals systems while confined to geometries more restrictive than bulk. The theory of operation, the sample preparation, and the electronic equipment involved in such measurements are described in detail. Examples of its use in heat capacity measurements of two-dimensional helium films at sub-Kelvin temperatures and in liquid crystal studies, a discussion on the simultaneously measured phase shift, which contains information regarding the order of the phase transition, is also included. © 1997 Elsevier Science B.V.

Keywords: Calorimetry; Phase Transitions; Superfluid; Helium; Liquid Crystals

1. Introduction

The study of phase transitions continues to be a research area of great interest. Thermodynamic measurements for accurately determining critical exponents are important as they allow to make connections to theoretical models. Although bulk studies continue to be of interest, with the recent advent of new manufacturing technologies, considerable research efforts have been devoted to the study of phase transitions in a variety of physical systems subjected to a wide variety of confining conditions. Typically, confinement is achieved by embedding the physical system in solid porous materials possessing cavities, either interconnected or isolated, of dimensions ranging from a few angstroms to several microns. To study phase transitions under such conditions and, in particular, to perform heat capacity measurements on the confined systems, a high-resolution technique capable of reliably extracting a small signal from a large addendum background is needed. As discussed in this paper, and as shown by several studies, AC calorimetry is ideal for such measurements.

Many reasons render AC calorimetry an extremely valuable tool in the study of phase transitions. The heat-capacity measurements essentially take place under quasi-equilibrium conditions. This is crucial, since much of the thermodynamic theory of phase transitions is based on equilibrium considerations. The technique also permits the implementation of averaging routines and total computer automation which

*Corresponding author. Tel.:+1 330 672 2994; Fax: +1 330 672 2959.

[1]Present address: Department of Chemistry, MIT, Cambridge, MA 02139.

PII S0040-6031(97)00183-4

are conducive to the resolution of sometimes remarkably small heat-capacity changes. In most cases, only a small amount of material is required to obtain the required to obtain the required high resolution. This is especially important both, to ensure thermal equilibrium as well as for those systems where a large sample may not be easily accessible, as for instance in the case of single-crystal high-temperature superconductors. Further, since the sample heating is typically produced by passing an electric current through a resistive wire, i.e. Joule heat dissipation, the absolute magnitude of the heat capacity is easily calculated. Very important for studies that take place below room temperature, which is difficult to achieve due to thermal radiation, a *strict* thermal isolation of the sample from the surrounding (as needed in an adiabatic calorimetry technique) is not required. Finally, the implementation of the technique is straightforward and easily adaptable for studying a variety of physical systems over a wide temperature range.

The ease of use and versatility of the AC calorimetry technique has been demonstrated by many studies on several different systems. Studies of the low-temperature properties of superfluid helium films adsorbed in porous glasses [1] and on graphite [2], superconducting films [3]; studies on the melting of nitrogen on graphite [4], and studies on phase transitions in bulk liquid crystals [5–9], and in free-standing liquid crystal films [10], are a few such examples published in the literature. The merits of the technique are hopefully further confirmed by the confined phase transitions studies presented here.

We highlight below the main features of the AC technique as used in our laboratory. In Section 2, we briefly discuss the theory of operation and include information regarding temperature calibration and control. General experimental details regarding the electronic instrumentation employed are presented in Section 3. In Section 4, typical data obtained using this technique in low-temperature heat capacity studies of two-dimensional helium films absorbed in interconnected Xerogel porous glass and in the parallel pores of Anopore membranes, which emphasize the different dimensionality behavior of the helium films according to the substrate's topology, are presented. In Section 5, we focus on liquid crystal studies at different-order phase transitions, including the second-order smectic-A-to-nematic (AN) and the weakly first-order nematic-to-isotropic (NI) phase transitions. Some of the results are compared with those obtained using a different calorimetric method on the system. A discussion of the phase shift signature and its relevance in the determination of the order of the phase transition is included. Concluding remarks are found in Section 6.

2. Theory of operation

2.1. Fundamental principles

The AC calorimetry technique was originally introduced by Sullivan and Seidel [11] in 1968. Briefly, in such a technique, a sinusoidal voltage heating of frequency f_v is applied to the sample of interest. In response, the sample exhibits temperature oscillation with a frequency $2f_v$. The heat capacity of the sample is inversely proportional to the magnitude of the induced temperature oscillations. The derivation of the heat capacity given below is independent of the geometry, i.e. the locations of the applied heat and the sensing of the resulting temperature oscillations are unimportant, provided that certain requirements are satisfied.

In Fig. 1, we show a thermal model for a sample whose heat capacity is to be measured. The systems consists of a heater (H) of the heat capacity C_H, and a thermometer (T) of heat capacity C_T, which are attached (glued) through thermal conductances K_H and K_T, respectively, to a supporting cell of heat capacity C_C. The sample of interest, of thermal conductivity K_S and whose heat capacity C_S is to be measured, is linked to the cell through a thermal conductance K_C. In most instances, these thermal conductances represent the boundary resistances for heat flow as in the case of the heat dissipated at the heater which flows through the attaching glue into the cell and, eventually, through the sample. The entire assembly: sample, cell, heater, and thermometer, of total (additive) heat capacity C, is thermally linked to an external temperature-regulated thermal bath via a conductance K_B. A heating $Q = Q_0(\cos(\omega_v t))^2$, where $\omega v = 2\pi f_v$ is the angular voltage frequency, is dissipated at the heater, inducing thermal oscillations of amplitude T_{AC} at an angular frequency, $\omega = 2\omega_v$. As

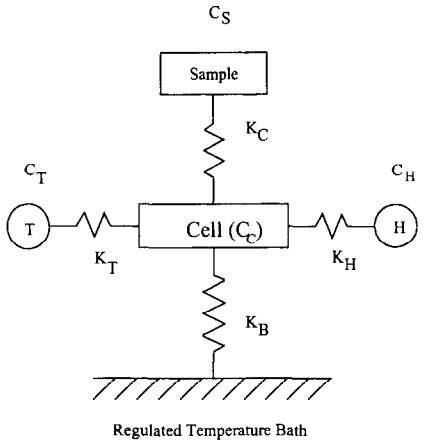

Fig. 1. Thermal model for the physical system showing the respective thermal links for the sample, thermometer, heater, and bath. The cell is assumed to have a negligibly small internal time constant, i.e. low heat capacity and high thermal conductance, and can be treated as a 'short'. The addendum heat capacity consists of the cell, heater, thermometer, and adhesives.

seen below, the amplitude of the temperature oscillations is related to the heat capacity.

The solution of the thermal equation for a one-dimensional model consisting of a planar sample of finite conductivity and total heat capacity C, is explicitly done in [12]. There, it is shown that the temperature as measured at the thermometer is given by:

$$T_T = T_B + \frac{Q_0}{2K_B} + \frac{Q_0}{2\omega C} \times \left[1 + \frac{1}{(\omega\tau_E)^2} + \omega^2(\tau_T^2 + \tau_H^2 + \tau_S^2 + \tau_C^2)\right]^{-1/2} \times \cos(\omega\tau - \alpha), \quad (1)$$

essentially consisting of DC and AC components. T_B is the regulated bath temperature; the second term in Eq. (1) is defined as $T_{DC} = Q_0/2K_B$ the sample temperature resulting from the rms heating; the last term represents the temperature oscillations induced by sinusoidal heating. The amplitude of these oscillations can be written in the form:

$$T_{AC} = \frac{Q_0}{2\omega C}\left(1 + \frac{1}{\omega^2\tau_E^2} + \omega^2\tau_I^2\right)^{-1/2}. \quad (2)$$

The thermal relaxation times have been defined as:

$$\tau_E = \frac{C}{K_B},\ \tau_T = \frac{C_T}{K_T},\ \tau_H = \frac{C_H}{K_H},\ \tau_C = \frac{C_C}{K_C}, \text{ and } \tau_S = \frac{C_S}{K_S}, \quad (3)$$

where we combined the individual time constants into $\tau_I^2 \equiv (\tau_T^2 + \tau_H^2 + \tau_C^2 + \tau_S^2)$, representing the total internal time constant of the thermometer, heater, cell, and sample, which is the time required for the entire assembly to reach equilibrium with the applied heat. The external time constant, τ_E, is the time required for the entire assembly to reach equilibrium with the thermally regulated bath. The cell is assumed to act like a 'short' for the heat: a point of high thermal conductance and low heat capacity; its associated time constant can be safely ignored in most circumstances.

From Eq. (1) it is seen that there is also a phase shift between the applied heat and the resulting thermal oscillations, α, which is given by:

$$|\tan\alpha| = \left(\frac{1}{\omega\tau_E} - \omega\tau_I'\right)^{-1}, \quad (4)$$

with $\tau_I' \equiv (\tau_\theta + \tau_H + \tau_S)$. The phase shift is related to both, the heat capacity and the thermal conductive properties of the entire system. Using Eqs. (3) and (4), and since the external time constant is typically temperature independent and can be separately measured via a frequency scan (see below), it is possible to solve for K_S, the sample thermal conductance. If the thermal conductances and heat capacities of the thermometer and heater are small and nearly constant, i.e. $B = \tau_T + \tau_H = \text{const}$, then, K_S may be written as:

$$K_S = C_S\left[\left(\frac{1}{\omega^2\tau_E} - B\right) - \frac{1}{\omega|\tan\alpha|}\right]^{-1}. \quad (5)$$

Hence, in addition to heat capacity measurements, information regarding the thermal conductance may be simultaneously acquired. This is of particular importance at phase transitions since ours and other researcher's work [13] have shown that there is a typical phase shift signature associated with the order of the phase transition.

Eq. (2) is an exact expression for the total heat capacity. However, by operating (heating) at a frequency such that the internal and external time con-

stants do not dominate T_{AC}, an approximation can be made which greatly simplifies the relation between T_{AC} and C. This approximation may lead to a small error in the absolute magnitude of the heat capacity but without loss of sensitivity to small changes. If the imposed oscillations are at a frequency 'slower' than the sample internal equilibration time (so that the sample achieves equilibrium with the applied heat), but 'faster' than the external equilibration time (so that a negligible amount of heat is lost to the bath), then, mathematically:

$$\frac{1}{\tau_E} < \omega < \frac{1}{\tau_I}, \tag{6}$$

which greatly simplifies Eq. (2), yielding for C:

$$C = \frac{Q_0}{2\omega T_{AC}} \tag{7}$$

Experimentally, it is feasible to fulfill the requirements of Eq. (6). The external time constant is controlled by tailoring the thermal link from the sample to the bath. It is usually made by thermally anchoring the heater and thermometer electrical leads to the temperature-controlled reservoir. This thermal link, of the order of 30 to 100 s, is adjusted by selecting the appropriate material, length and cross section of the leads. All of these choices depend on the temperature regime of the measurements.

Adjustment of the internal time constant is not so straightforward as it mostly depends on the thickness of the sample (the time constants of the thermometer and heater links are again neglected). If the sample thickness is less than the thermal diffusion length given by:

$$l = \sqrt{\frac{2K_S A}{\omega C_S}} \tag{8}$$

where A is the cross-sectional area of the sample, then, the right-hand side inequality of Eq. (6) is satisfied. If Eq. (6) holds, the locations of the heater and thermometer on the cell become unimportant, and the measurement is now independent of the geometry, Finally, note that the heat capacity increases linearly with thickness (mass) while the thermal conductance varies as the inverse of the thickness L. For instance, the internal time constant for a sample, half as thick, is a factor of four shorter, which will lead to a higher operational heating frequency.

Experimentally, the thermal requirements expressed in Eq. (6) need to be verified for every sample by means of a frequency scan. A frequency scan essentially determines the frequency regime over which the measured heat capacity will be frequency-independent. Such a frequency profile is experimentally obtained by maintaining the same voltage amplitude oscillations to the heater and keeping the bath temperature constant while sweeping the frequency and measuring the resulting sample temperature oscillations at every frequency. For a well-designed cell, a plot of $f_v T_{AC}$ vs. f_v should show a nearly horizontal region, a 'plateau'. The plateau indicates the region where the heat capacity will be frequency-independent (and also gives the smallest heat capacity) and, thus, neither thermal relaxation time, external or internal, plays a major role and can be neglected in the calculation. Alternatively, one can plot T_{AC} as a function of $(2f_v)^{-1}$, which would exhibit a straight line region passing through the origin. If operation is within this region, the requirements of Eq. (6) are satisfied.

A typical frequency scan from our liquid crystal work is shown in Fig. 2; the wider the plateau, the smaller the error associated in calculating C from the simplified Eq. (7). In the example shown, the time constants are $\tau_E = 31.4$ s and $\tau_I = 1.26$ s, corresponding to roll-off frequencies of 0.032 and 0.79 Hz, respectively. Comparing C as calculated from Eq. (7) rather than from the full expression of Eq. (2), for the particular example of Fig. 2, introduces an error in the absolute magnitude of the heat capacity of 3.8% at 100 mHz; much larger errors in the absolute magnitude would exist if operations were near the roll-off frequencies.

Since Joule heating is dissipated at the heater of resistance R, and if V_P is the peak voltage, the power dissipated at the heater is given by $Q_0 = P_P = (V_P)^2/R = P_{PP}/4$, where $P_{PP} = V_{PP}^2/R = 2(V_P)^2/R = 4V_P^2/R$ is the peak-to-peak power. Substituting in Eq. (7) together with $\omega == 2\pi f = 4\pi f_v$ and $T_{AC} = \sqrt{2}T_{AC}(\text{rms})$, C can be case in the form:

$$C = \frac{P_{PP}}{32\sqrt{2}\pi f_v T_{AC}(\text{rms})}. \tag{9}$$

The amplitude of the temperature oscillations was converted to an rms value since, in our setup,

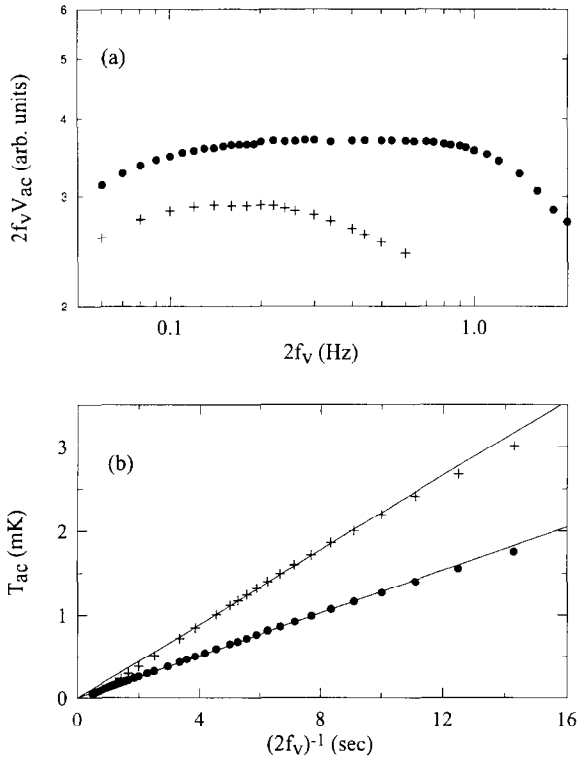

Fig. 2. Typical frequency scans for the liquid crystal (•) – empty calorimeter and (+) – with a sample present. Log–log and linear constructions are shown.

they are measured using a lock-in amplification technique.

In an actual measurement, the addendum heat capacity consisting of the contributions from the cell, thermometer, heater and adhesives, is first measured and then subtracted from a subsequent measurement with the sample present. In the current example, the addendum heat capacity is 42 kJ/K at 303 K, increasing to 46 mJ/K at 317 K. As with any other heat capacity measuring technique, the addendum heat capacity should be kept to a minimum in order to maximize sensitivity. This is probably more important in the AC technique as a large addendum may lead to a lack of a frequency plateau, or, shift the plateau to frequencies below the capabilities of a lock-in amplifier (see Fig. 2); measurements would then require signal digitization. The latter is not a major drawback as evidenced by the high-resolution results of Garland et al. [13] at MIT

2.2. Thermometry

An accurate measurement of the temperature oscillations is the primary ingredient in the determination of the heat capacity. In our setup, such oscillations are detected with a resistor (that serves as the thermometer) which is DC biased, with a constant current I. The absolute temperature is obtained by calibrating the thermometer, usually $T = f(R)$, or, equivalently, due to the DC bias, as a function of voltage, i.e. $T = f(V)$. Differentiating, we obtain $dT/dR = df(R)/dR = g(R)$, or, $dT = g(R)dR$. In the limit of small temperature oscillations, one can approximate $T_{AC} \cong dT$. The 'constant' temperature about which the sample is oscillating is determined from $f(\langle R \rangle)$, where $\langle R \rangle$ is the average resistance of the thermometer. In terms of the measured voltage drop across the thermometer, $V_{DC} = I\langle R \rangle$, the previous analysis yields $dR = dV_{DC}/I$, or, $dT = g(V_{DC}/I)V_{AC}/I$, where we have identified $dV_{DC} \cong V_{AC}$.

The function $f(R)$ needs to be empirically determined for each sensor used. For carbon flake thermistors which are useful in room temperature studies, we have found that:

$$\frac{1}{T} \equiv \sum A_n \ln(R)^n = A_0 + A_1 \ln(R) + A_2 \ln(R)^2 + \cdots \quad (10)$$

works rather well. Over the same temperature range, a platinum thermometer satisfies the equality $T = \sum A_n R^n$. The best fit is chosen as the one with the lowest chi-square, using the least number of coefficients, often ranging between four and seven. Clearly, the largest number of coefficients that can be used depends on how many data points are available in the actual temperature calibration.

Speer or Allen-Bradley carbon thermometers, useful at liquid helium temperatures, are calibrated against a factory calibrated germanium thermometer as a function of voltage for several different bias currents. Several currents are used according to the temperature range to avoid the thermometer self-heating (Joule heating) at low temperatures while maximizing its sensitivity at higher temperatures (> 1 K), where dR/dT decreases sharply. Measurements obtained employing different currents are overlapped and scaled to produce a single calibration. Although many alternatives exist, carbon resistors

are usually fit to a polynomial of the form $\ln(T) = \sum A_n(\ln(V))^n$.

For the room temperature sensors employed in the liquid crystal studies, since the induced temperature oscillations are obtained from the derivative of the temperature, from Eq. (10) we obtain

$$dT \cong T_{AC} = \frac{T^2 V_{DC}}{R_{th} I}[A_1 + 2A_2 \ln(R_{th}) + 3A_3(\ln(R_{th}))^2 + \cdots] \quad (11)$$

where $R_{th} \equiv \langle R \rangle$ for the thermistor and T is the temperature given by Eq. (10). Substitution of Eq. (11) in Eq. (9) leads to a final operational expression that allows to calculate the heat capacity in terms of all measurable quantities:

$$C = \frac{P_{PP} I R_{th}}{32\sqrt{2} T^2 V_{AC} \pi f v}[A_1 + 2A_2 \ln(R_{th}) + 3A_3 \ln(R_{th})^2 + \cdots]^{-1}. \quad (12)$$

where a factor of $\sqrt{2}$ has been included to convert V_{AC} value from peak to rms.

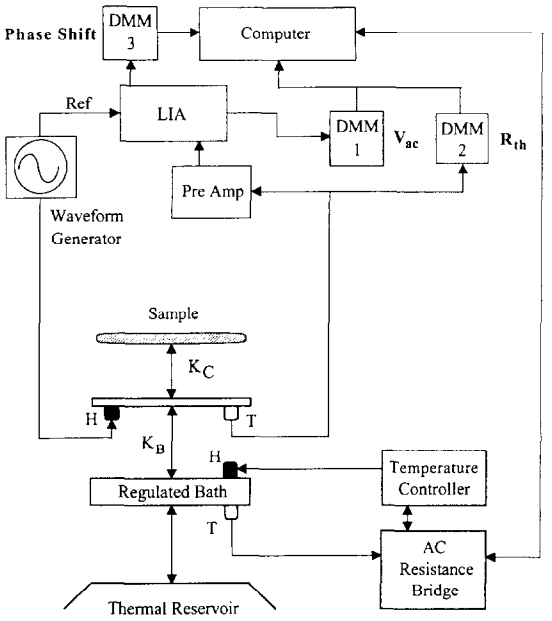

Fig. 3. Schematic diagram showing the electronic instrumentation and connections. LIA – lock-in amplifier, and DMM – digital multimeters.

3. Electronic instrumentation

A block diagram of the electronic equipment used in our application of the AC calorimetry is shown in Fig. 3. The cell, weakly anchored to the bath regulated at a temperature T_B, is provided with a resistive heater to induce small temperature oscillations on the sample while raising its average temperature by an amount $\Delta T = T_{DC}$ above the bath. The magnitude of these oscillations is detected by the cell resistive thermometer. Scanning the cell temperature by changing the temperature of the bath, one obtains the heat capacity of the sample as a function of temperature.

Temperature control is extremely important. In our work, the regulated temperature stability of the bath is of the order of 70 μK for the liquid crystal work, and of the order of a few μK at liquid helium temperatures. Resistance thermometry provides the simplest and most convenient measurement and control of temperature. We have achieved the necessary temperature regulation using several resistance bridges/temperature controllers combinations such as Quantum Design digital R/G bridge model 1802 [14], Lakeshore temperature controller model DRC-93C [15], and the Linear Research AC-resistance bridge/temperature controller models LR-400/LR-130 combination [16]. We have also employed homemade AC resistance bridges (Wheatstone type) using a ratio transformer and a lock-in amplifier as the null detector. These provide excellent temperature stability and sensitivity for a variety of sensors, including carbon flake thermistors [17], platinum thermometers [15,18], germanium resistors [15], and ruthenium oxide resistors [18]. These controllers offer different computer control programming feature; all of them use proportional–integral–derivative (PID) control action [19], eliminating set point offset, deviation, and overshoot. The success in temperature control lies in using a high resolution and fast responding thermometer, while simultaneously locating the heating element in its neighborhood on a 'bath' constructed from high thermal conductivity materials.

The cell-thermometer temperature has been measured in two ways, both involving a DC current bias. The first method uses a digital multimeter in resistance mode, thus naturally applying a constant excitation current to the thermometer for its resistance measure-

ment. Although of excellent current stability, in some cases, it may require an expensive seven-and-a-half digits multimeter in order to have high resolution at low excitation currents. Further, the range of available currents is often limited or changes steps that may be too large. The second method involves the construction of an external current source. This is done using mercury batteries and metal film resistors which allows customization of the bias current. Mercury-battery operated current sources have the added advantage of isolation from the line of 60 Hz noise. For low-temperature work, we built a current source with ten different current settings between 9 and 350 nA. The voltage drop across the sensor can then be read with an inexpensive voltmeter. We have used digital multimeters from Hewlett–Packard [20], Keithley Instruments [21], and John Fluke [22]. They are all versatile, reliable and offer ease of computer control programming and interfacing option. Other features include internal noise filtering, signal averaging and five-to-seven digit accuracy. As mentioned earlier, whether using a multimeter in resistance mode or a current source, care should be taken in minimizing the thermometer self-heating to avoid erroneous absolute temperature readings. This problem, obviously a greater concern at low temperatures, can be alleviated by keeping the power dissipated at the cell thermometer a factor of 100 to 1000 smaller than the power dissipated at the cell heater.

To induce thermal oscillations, we use a waveform generator operating at the proper frequency (as determined from a frequency scan) and a peak-to-peak voltage set to produce the desired amplitude size of temperature oscillations. Wavetek [23] signal generators have proven to be very stable in amplitude and frequency. The magnitude of the temperature oscillations is dependent on how strong a function of temperature is the heat capacity of the sample. Away from a transition, one can afford larger oscillations than near a transition where, due to the rapid changes in heat capacity with temperature, rounding and a non-reliable averaged heat capacity magnitude would be introduced. In all events, it is a good practice to keep the temperature oscillations at a minimum.

The signal from the thermometer consists of a DC voltage (typically in the millivolt range) mixed with microvolt size AC oscillations. The DC component is directly read and averaged with a multimeter, yielding the absolute temperature ($\langle R \rangle$ or V_{DC}). This signal is also fed to a pre-amplifier, where the DC component is removed while the AC component is amplified and filtered. We use a low noise EG&G 113 pre-amplifier [24] that provides user-adjustable linear amplification with selective high- and low-frequency roll offs. The choices of roll offs allow the amplifier bandwidth to be narrowed about the range of interest, increasing the stability of the signal output. The amplified signal is then fed to a low-frequency lock-in amplifier operating at 40 or 100 s time constant (depending on the frequency) for better signal averaging. The reference signal for the lock-in amplifier can be provided in one of four ways: splitting the signal generator output driving the cell heater, the signal generator TTL output, a separate signal generator or the internal oscillator of the lock-in. For the first two methods, the lock-in must operate in $2f$ mode. The last two methods require the reference to be in phase with the applied power signal, in which case the lock-in operates in the $1f$ mode. We typically use the TTL output of the generator and the $2f$ mode of lock-in operation.

We have used an Ithaco 399 (Ref. [25]) and EG&G 5210 dual-phase lock-in amplifiers. The main difference between these models is the limiting low-frequency detection. The Ithaco has a low-frequency limit of 0.05 Hz as compared to 0.5 Hz for the EG&G. The latter, a digital lock-in amplifier, includes GPIB interfacing and offers a wide range of computer controllable parameters. The Ithaco requires an additional coupler to achieve similar computer control. A recently available, but expensive digital lock-in amplifier, EG&G 5302, may now be used to frequencies as low as 1 mHz. For our more recent work, we started using the inexpensive Stanford 8530 digital lock-in amplifier. We have found it extremely stable and reliable to frequencies as low as 10 mHz. The Standard lock-in has also yielded the highest resolution and larger signal-to-noise phase shift data.

The in-phase output of the lock-in is averaged with a multimeter (usually an HP 5428) and provides the magnitude of the voltage oscillations, V_{AC}, which are proportional to the temperature oscillations T_{AC}. The out-of-phase output of the lock-in amplifier is also averaged with a multimeter, and it is a measure of the phase shift, α, between the applied and induced oscillations.

The central component of the system is the computer. It is responsible for signal averaging, data storage and automation of the entire system through the GPIB (IEEE-488) standard interface. Specific duties, such as temperature control and voltage or resistance measurements, are left to specific devices.

An actual data point measurement proceeds as follows. After waiting a specified time for the system to come to equilibrium with a new bath temperature, and, allowing the lock-in amplifier to stabilize, averaging begins on R_{th} and V_{AC} in blocks equivalent to one or two time constants of the lock-in. A block average is compared to the previous block average and if the difference between them is within custom specified limits, 0.01 to 0.03%, then, the data taking routine starts. Otherwise, the process of block averaging repeats until stable conditions are achieved. The strictness of the specified limits depends on the long-term drifts associated with a particular experimental setup. The data-taking routine continues the averaging of R_{th}, V_{AC} and α over a specified number of points. Each point corresponds to one reading of R_{th}, V_{AC} and α. Once completed, the averages are saved to a file, a new bath temperature set and the process repeated. Depending on the application, 3000 data points are averaged after a 5 to 10 min wait. Data is taken at points 10 mK apart, or less if close to a transition. At low temperatures, more closely spaced data can be easily obtained. Given the thermal characteristics, computer speed is unimportant. A 286/12 MHz computer with math co-processor more than satisfies any speed requirements.

Many programming languages allow user-defined graphics windows for plotting numerical input. We simultaneously display each device output, monitoring the experiment progress in numerical and graphical format. Our control program also has an interrupt feature which allows the user to manually operate the experiment.

4. Superfluid-films heat capacity studies

4.1. Helium films in Anopore membranes

The temperature range appropriate for this type of work is 0.05–2 K and is achieved with a dilution refrigerator. The calorimeter was constructed as follows. For the cell-temperature sensor, we used carbon resistors such as Speer™, Allen-Bradley™ and Matsushita™, as well as electrically conducting carbon paint, Electrodag 501 [26–28]. These sensors provide the necessary sensitivity and reproducibility as long as they are kept at low temperatures (< 77 K). It is common practice to shave down carbon resistors and remove the bakelite coating to reduce their heat capacity contribution.

A major concern in low-temperature work is the self-heating of the resistance sensors. To minimize it and to obtain a fiducial absolute-temperature reading, the power dissipated at the cell thermometers is typically in the nW–pW range. In addition, we found that commercially available current sources introduce unwanted ground loops, causing the thermometry to be noisy. Instead, as discussed earlier, mercury battery powered DC current sources employing high resistance metal film resistors were built and several current levels in the nA range were easily obtained.

A typical experimental cell for helium films studies, sketched in Fig. 4, has to be vacuum-tight. It consists of inner and outer brass-shim cups, 2.1 cm in diameter and 0.05 mm thick, fitting snugly inside each other. The substrate onto which helium films are adsorbed, aluminium oxide Anopore membranes [29] are disks, 60 μm thick, with 0.2 μm diameter parallel cavities. Several Anopore disks are stacked, one above the other, within the brass cups. The cell is sealed along the edge with Emperson Cummings 2850 epoxy [30]. Helium is admited to the cell through a 0.15 mm I.D., 46 cm long coiled cupronickel (or stainless steel) capillary previously soldered to one face of the cell. The heater is made of 28 Ω/cm Evanohm™ wire, 18 cm long, glued with GE varnish [31] to the opposite face of the cell. Its electrical connection is made with 0.03 mm diameter copper leads providing an external time constant ranging between 20 and 50 s, mostly depending on the heat capacity of the sample. The thermometer, glued with GE varnish to one face of the cell, is a shaved down (0.8 mm thick) Speer carbon resistor with a nominal room-temperature resistance of 470 Ω. After shaving, it reads 800 Ω. The Speer thermometer was calibrated against a calibrated Lakeshore Cryotronics germanium resistance thermometer anchored at the platform, using several DC bias currents between 37–495 nA over the 0.1–2 K temperature range. Its electrical connections are two

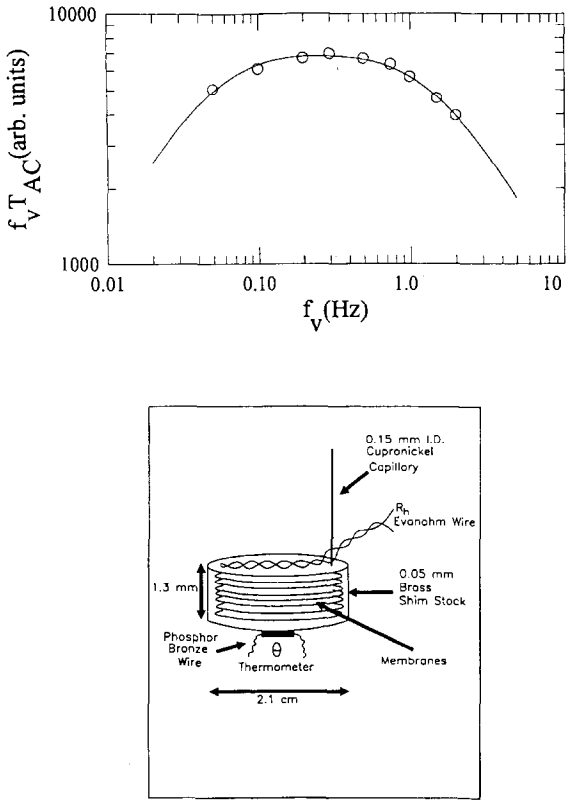

Fig. 4. (Top) Frequency scan for the low-temperature helium studies. (Bottom) Sketch of the heat capacity cell used to study two-dimensional helium films in Anopore membranes.

0.05 mm-diameter phosphor bronze leads. Phosphor bronze is used because of its poorer, than copper, thermal conductivity and hence it does not add and shorten the overall external time constant. Although the feed capillary, thermometer and heater leads are all thermally anchored to an experimental platform (regulated bath) in the refrigerator, the main thermal link is through the heater leads. The data shown here was obtained with f_v from 0.05 to 1.0 Hz range, μW power dissipated at the cell heater and nA DC bias of the cell thermometer. The induced oscillations ranged between 10 and 1000 μK.

To determine the operating characteristics of the calorimeter, power was applied to the cell. The helium sample cell temperature was kept ≈50 mK above the regulated bath (here an oxide-free high conductivity platform attached to the mixing chamber of the dilution refrigerator) temperature, T_B. By changing the voltage frequency, a plateau extending from 0.7 to 5 Hz was found. The frequency scan (an example is included in Fig. 4) was repeated at several temperatures in the temperature range of measurements and an operating frequency chosen. In some cases, usually when a large heat capacity peak was present, two or more frequencies were used to scan the peak. Data taken at different frequencies was extensively overlapped to insure a perfect matching.

Having established the operating frequency, the cell is cooled to the lowest temperature, namely 0.1 K. Power into the cell is gradually applied until there are measurable thermal oscillations induced in the cell. The temperature of the cell is then changed by gradually increasing the regulated bath platform temperature. Since the heat capacity of helium films increases rapidly with temperature and the oscillation amplitude consequently decreases, more power is applied. Again, data taken at different powder levels is overlapped. If the amount of helium in the cell is changed to produce a different film thickness, frequency scans were repeated, and as needed, a different operating frequency used. It is customary for a heterogeneous media to report the thickness in terms of helium coverage per unit area, or μmol/m^2.

Prior to condensing a known amount of helium gas in the cell to form the film, the addendum heat capacity was measured. This configuration has a total addendum heat capacity of 4.5 μJ/K at 0.5 K. Heat capacity data was taken from 0.1 to 2 K and, depending on the features observed, data was spaced every 2–5 mK or 30–50 mK. A selection of the heat capacity results for helium films, whose thickness is labeled by the amount of helium condensed divided by the surface area of the porous substrate, confined in the 0.2 μm cylindrical pores of Anopore membranes are shown in Fig. 5 over a narrower temperature range. Although not fully appreciated from the figure, 1% changes above the addendum are reliably resolvable given the 0.1% data scatter. The data shown illustrates the high resolution of the technique.

Note that these helium films are essentially planar since their thickness, < 1 nm for all cases shown, is much less than the Anopore 0.1 μm pore radius, thus, they should exhibit features predicted by the Kosterlitz–Thouless theory [32,33]. The large, broad and round heat capacity peak shown, is centered at a temperature above the superfluid-to-normal transition

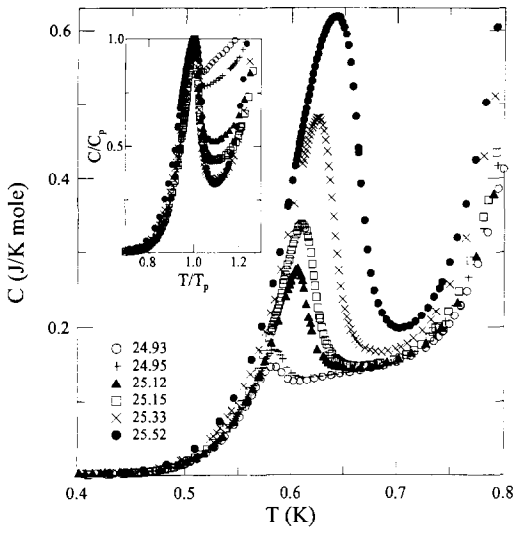

Fig. 5. Heat capacity results for several ^{4}He films adsorbed in Anopore membranes. The inset shows the same data scaled by the peak maximum and temperature position. Numbers refer to the amount of helium in the cell divided by the surface area, μmol/m^2. The broad peak is the expected vortex–antivortex unbinding peak.

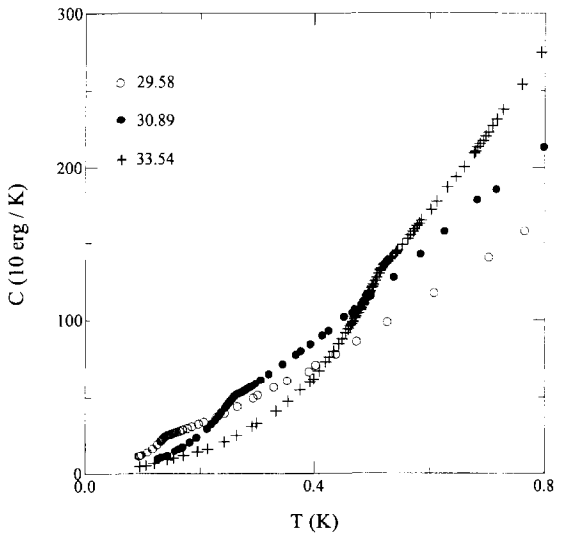

Fig. 6. Heat capacity results for helium adsorbed in Vycor glass. The heat capacity signature is coincident with the superfluid-transition temperature. Numbers refer to the film thickness in μmol/m^2.

temperature, and is a manifestation of the expected vortex–antivortex unbinding mechanism that signals the destruction of the superfluid behavior. Also note that the data can be easily made to collapse on a single curve, shown in the inset to Fig. 5, suggestive of a universal mechanism, independent of film thickness.

4.2. *Helium films in Xerogel porous glass*

The confinement of helium films to multiply connected geometries such as porous glasses received renewed experimental and theoretical attention in the late eighties. The major reason was that superfluid density measurements of helium films in porous Vycor glass (pore diameter 7 nm) reveal a sharp transition at T_C with an asymptotic power-law dependence similar to the bulk lambda transition. These results suggested that helium films in Vycor belong to the same universality class as bulk helium and, thus, it was expected that the heat capacity of films in Vycor would exhibit an anomaly at the superfluid-to-normal transition.

Several attempts, but none using an AC calorimetry technique, at measuring the specific heat of films in Vycor failed to reveal a sharp anomaly at T_C until Finotello et al. at Pennsylvania State University used the AC calorimetry technique to study this system [34].

The experimental cell consisted of a thin piece of Vycor class, ≈9 mm in diameter and 0.6 mm thick, that was fully coated with a thin layer of 2850 Stycast epoxy. Because of the smallness of Vycor pore size and the viscosity of the epoxy which was applied shortly prior to being fully cured, little epoxy penetrated the pores. The cell was completed by also gluing with epoxy an Evanohm heater and painting an Electrodag carbon thermometer. The AC technique was employed as described here and the results for a few selected films are shown in Fig. 6.

The results, presented in Fig. 6, represent the first observation of a small yet sharp signature in the heat capacity of helium films in porous glass. The temperature position of the heat capacity signature coincides with the superfluid-transition temperature as determined by independent superfluid density measurements. This is suggestive of the superfluid transition in porous media as being a phase transition with genuine critical behavior. This is in contrast with the earlier Anopore results where the peak was centered not at T_C, but at a higher temperature, reflecting the

film's different dimensionality behavior. In both cases, much of the success of the measurements can be attributed to the use of the AC technique.

5. Liquid crystal phase transitions

The high temperature calorimeter, shown in Fig. 7, is designed for versatility and ease of liquid crystal sample placement. A solid brass cylinder is machined such that there is a concentric cylindrical cavity with one open end creating a 'ring'. The temperature of this ring is the regulated 'bath' temperature. Penetrating from the closed end are the electrical connections for the thermometer and the heater. The open end is sealed with a brass cap. A cavity is drilled in the ring wall, parallel to the cylinder axis, and a calibrated, 100 Ω platinum thermometer, is snugly fitted. Wrapped around the exterior of the ring is a resistive (manganin) heater wire. This ring is supported by a 0.3 cm diameter, 4 cm long brass post which provides the thermal link to a larger, evacuated copper chamber. This chamber is rested on a large aluminum block, partly submerged in a water bath. With this configuration, we have been able to obtain reliable data over the 25–125°C temperature range. Below room temperatures may be achieved using a TED (thermoelectric device) placed between the copper can and the aluminum block.

The calorimeter cell consists of a 10 kΩ carbon flake thermistor and a 50 Ω Evanohm heater attached to the same side of a 10 mm diameter, 0.1 mm thick sapphire disk. Sapphire was chosen for its rigidity, flatness, high thermal conductivity, and low heat capacity at room temperature. It is also compatible with many solvents allowing thorough surface cleaning before sample placement. The thermistor flake has the advantage of its extremely small size, < 0.05 mm on side, which allows a quick response to temperature changes, i.e. a short internal time constant. Small amounts of adhesive, such as GE varnish or 1266 Stycast epoxy [30], are used to attach the thermistor and heater to the sapphire disk. This minimizes the

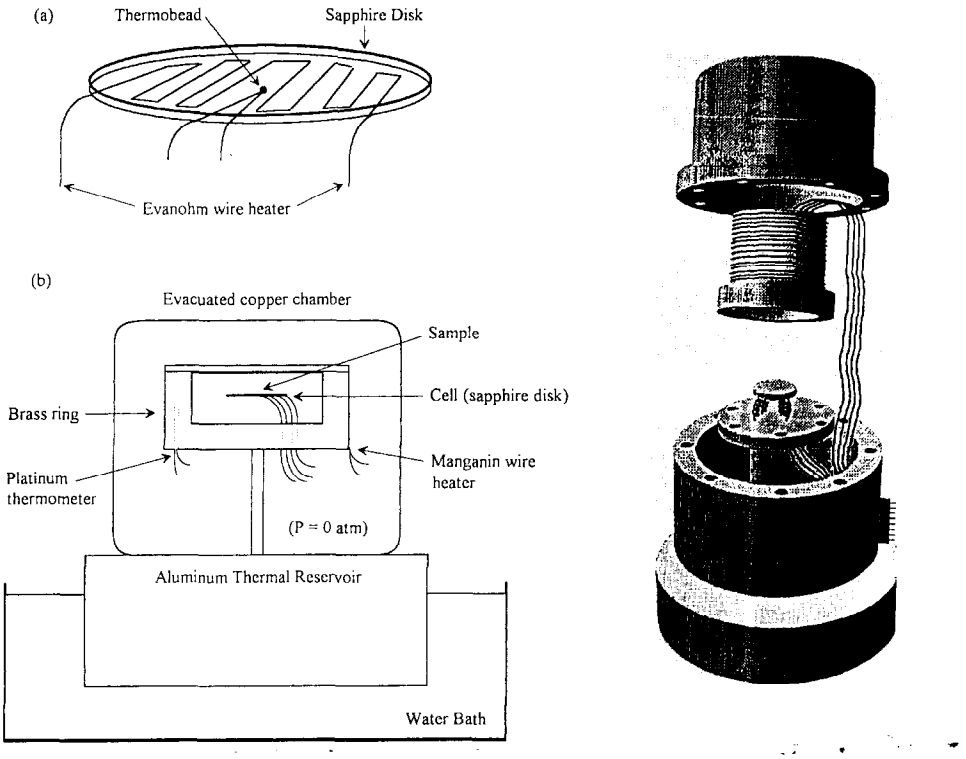

Fig. 7. Schematic and artistic conception of the liquid crystal calorimeter.

addendum heat capacity while ensuring good thermal contact. The temperature sensor, heater, and sapphire disk arrangement has an internal time constant of ≈1.26 s (a high frequency roll off of 0.79 Hz). Attempts with larger thermistors resulted in internal time constants longer than the external time constant, giving an unacceptable frequency profile, i.e. no plateau. The heater and thermistor leads are thermally anchored to the ring. The length of the leads from the sapphire disk to the ring, and their cross-sectional area, control the external time constant. Here, copper leads, 25 mm long and 0.22 mm in diameter, giving an external time constant of ≈31.4 s (a low frequency roll off of 0.032 Hz) were used. The applied voltage frequency was 0.055 Hz and the induced temperature oscillations were ≈2 mK in amplitude. With 10 mK steps in temperature, a wait time of 7 min and averaging for 8 min at each temperature, a relative resolution of 0.2% or better in heat capacity is achieved.

An example of heat capacity measurement for bulk 8CB, a thermotropic liquid crystal that undergoes a second-order smectic-A-to-nematic, and a weekly first-order nematic-to-isotropic phase transition, is shown in Fig. 8. The measurement was performed using < 9 mg of liquid crystal material, forming a droplet and rested directly on top of the sapphire disk, opposite to the thermistor and heater. The liquid crystal was allowed to spread naturally over the sapphire, so it was estimated that the drop had a thickness of 0.2 mm over an 8 mm diameter. The system was cycled in temperature several times to ensure complete settling of the material onto the disk. Comparing with results of Ref. [9], where measurements in a highly sophisticated, high-resolution adiabatic scanning calorimeter required 21 g of material, comparable data quality was obtained with 10^3 less mass. Although we seem to measure a smaller peak at the smectic-A-to-nematic transition, it is merely a consequence of the large spacing (10 mK) among consecutive data points. After analyzing these data for critical behavior, identical critical exponents to those quoted in [9] were found to within experimental error. This clearly demonstrates the remarkable sensitivity of this technique using very little material. In general, we have successfully resolved liquid crystal phase transitions, both for bulk and under confinement, using roughly 2 mg of material [33,36].

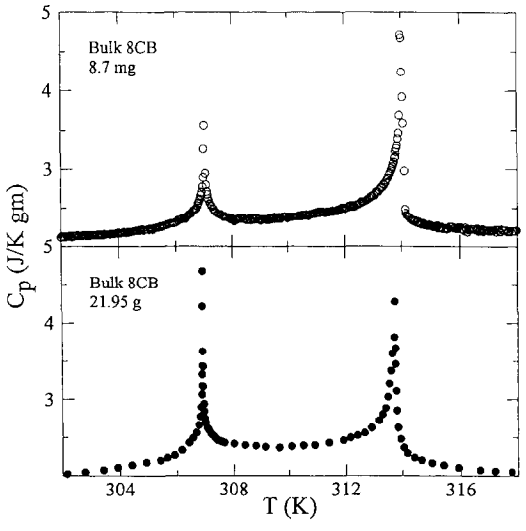

Fig. 8. Specific heat results for bulk 8CB liquid crystal from this work (top) and that of Ref. [9] (bottom).

The phase shift change, $\Delta\alpha$, contains information regarding the order of a phase transition. The behavior of the phase shift, for a different sample (9.01 mg) of bulk 8CB than that shown in Fig. 8, is presented in Fig. 9. At the weakly first-order nematic-to-isotropic phase transition, there is typically a very sharp peak in $\Delta\alpha$, almost coincident with the observed heat capacity peak. This has been interpreted as the region of coexistence of two phases for a first-order transition in the sample. For a second-order phase transition, there is most often a decrease in $\Delta\alpha$, presumably due to the absence of latent heat and a correlation length diverging to macroscopic-length scales. Indeed, at the smectic-A-to-nematic phase transition of 8CB, we find a very small decrease in the phase shift, consistent with the second order nature of this transition.

The usefulness of the simultaneous acquisition of the phase shift is further seen from our liquid crystal confined studies. In Fig. 10, we show specific heat results for bulk 8CB as well as 8CB confined to the interconnected voids of Millipore filter paper. With decreasing void size, the NI transition is not too distinct from bulk, except for some broadening representative of a wider region of coexistence. In contrast, the AN transition is considerably suppressed by the random confinement [35]. The Millipore effects at these transitions are somewhat similar to those found in the well-defined Anopore geometry [36].

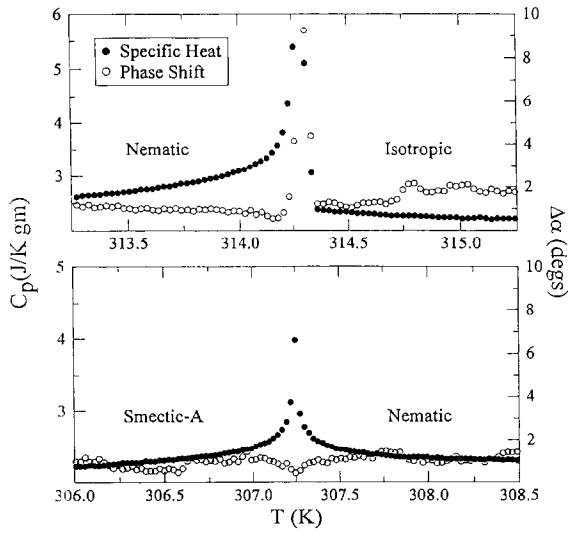

Fig. 9. Specific heat and phase shift, $\Delta\alpha$, between the applied heat and the induced temperature oscillations and heat capacity for bulk 8CB at the weakly first-order nematic-to-isotropic phase transition (above) and the second-order smectic-A-to-nematic phase transition (below).

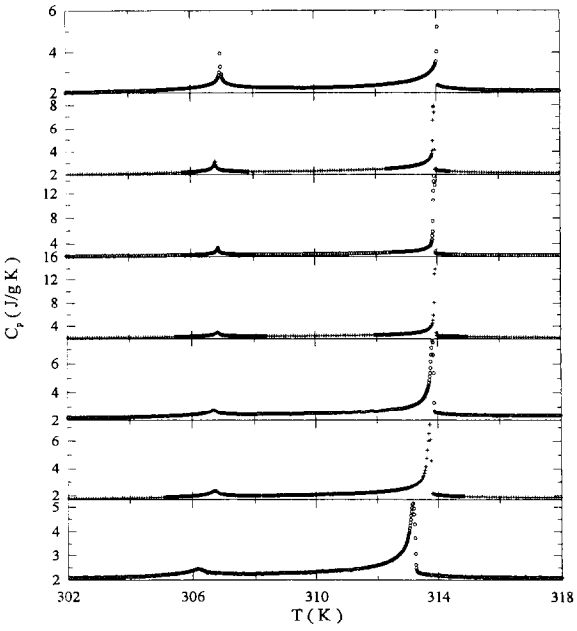

Fig. 10. Specific heat of bulk 8CB and confined to Millipore filters. The void sizes, in descending order, are 5, 0.8, 0.22, 0.1, 0.05, 0.025 μm.

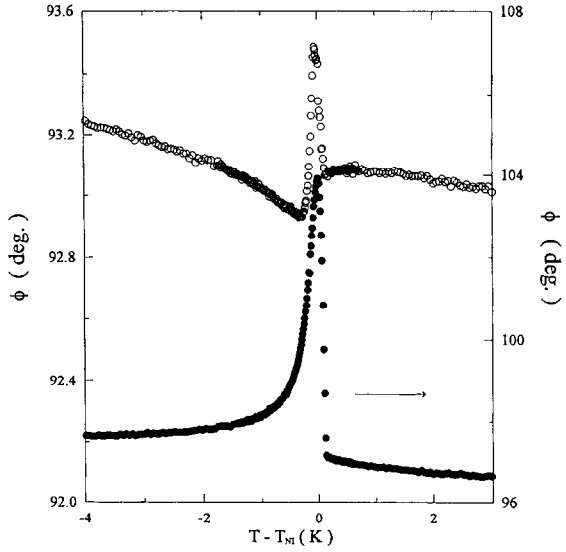

Fig. 11. Phase shift behavior at the NI transition in (o) – Anopore and (•) – 5 μm Millipore.

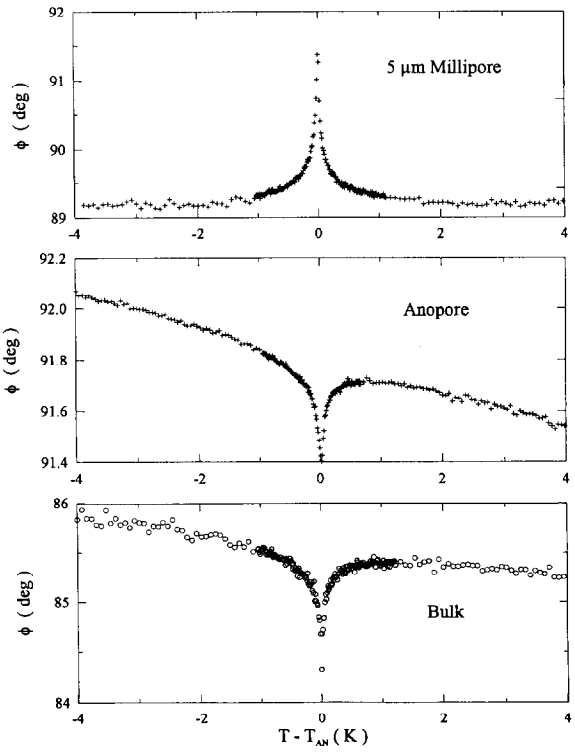

Fig. 12. Phase shift behavior at the AN transition for 8CB, bulk and confined to Millipore and Anopore.

However, examination of the phase shift results points out similarities as well as significant differences between the two confining materials. At the NI transition, Fig. 11, the phase shift signature in both Millipore and Anopore is a peak, reminiscent of the specific heat peak. This behavior is identical to that of the bulk material that was shown in Fig. 9. In contrast, at the AN transition, the phase shift signature in Anopore is just like in bulk, while in Millipore it is remarkably different: instead of a dip, a symmetric peak is obtained as seen in Fig. 12. This latter result led to a careful data analysis from which it was concluded that the Millipore confinement weakens the coupling between smectic- and nematic-order parameters, thus drastically changing the critical exponents [35].

6. Conclusions

We have presented an overview of the AC calorimetry and demonstrated its versatility by providing example of studies that were performed at very different temperature regimes. The greatest advantage of the technique is its sensitivity at near equilibrium conditions. We have shown that with computer averaging and lock-in amplification detection, a high resolution requiring only small samples is achieved. The latter may be important for certain systems, where large masses are not available, as for instance single crystal high temperature superconductors.

Acknowledgements

We benefited from discussions with Moses Cha, Carl Garland and David Johnson. This work was supported by the NSF Science and Technology Center ALCOM Grant DMR 89-20147.

References

[1] Y.P. Feng, A. Jin, D. Finotello, K.A. Gillis and M.H.W. Chan, Phys. Rev., B38 (1988) 7041.
[2] H.B. Chae and M. Bretz, J. Low Temp. Phys., 76 (1989) 199.
[3] T.W. Kenny and P.L. Richards, Rev. Sci. Instrum., 61 (1990) 822.
[4] H.K. Kim, Q.M. Zhang and M.H.W. Chan, Phys. Rev. Lett., 56 (1986) 1579.
[5] J.E. Smaardyk and J.M. Mochel, Rev. Sci. Instrum., 49 (1978) 988.
[6] C.A. Schantz and D.L. Johnson, Phys. Rev., A17 (1978) 1504.
[7] D.L. Johnson, C.F. Hayes, R.J. DeHoff and C.A. Shantz, Phys. Rev., B18 (1978) 4902.
[8] J.D. LeGrange and J.M. Mochel, Phys. Rev., A23 (1981) 3215.
[9] J. Thoen, H. Marynissen and W. van Dael, Phys. Rev., A26 (1982) 2886.
[10] R. Geer, T. Stoebe, T. Pithford and C.C. Huang, Rev. Sci. Instrum., 62 (1991) 415.
[11] P.F. Sullivan and G. Seidel, Phys. Rev., 173 (1968) 679.
[12] H.S. Carslaw and J.C. Jaeger, Conduction of Heat in Solids, 2nd edn., Oxford Press (1959).
[13] X. Wen, C.W. Garland and M.D. Wand, Phys. Rev., A42(10) (1990) 6087.
[14] Quantum Design, 11578 Sorrento Valley Rd. suite 30, San Diego, CA 92121.
[15] Lakeshore Cryotronics Inc. 64 E. Walnut St. Westerville, OH 43081.
[16] Linear Research Inc. 5231 Cushman Pl. Suite 21, San Diego, CA 92110.
[17] Thermometrics Inc. 808 U.S. Highway 1, Edison, NJ 08817.
[18] Scientific Instruments Inc. 4400 West Tiffany Dr. Magonia Park, FL 33407.
[19] C.L. Nachtigal, Instrumentation and Control Fundamentals and Applications, John Wiley and Sons (1990).
[20] Hewlett–Packard Co., 5201 Tollview Dr., Rolling Meadows, IL 60008.
[21] Keithley Instruments Inc., 28775 Aurora Rd., Cleveland, OH 44139.
[22] John Fluke Mfg. Co. Inc., PO. Box 9090, Everett, WA 98206.
[23] Wavetek San Diego Inc., 9045 Balboa Ave., San Diego, CA 92123.
[24] EC&G Princeton Applied Research, PO. Box 2565, Princeton, NJ 08543.
[25] Ithaco Inc., 735 West Clinton St. Box 6437, Ithaca, NY 14851.
[26] G.K. White, Experimental Techniques in Low-Temperature Physics, 3rd edn., Oxford Science (1979).
[27] R.C. Richardson and E.N. Smith, Experimental Techniques in Condensed Matter Physics at Low Temperatures, Addison–Wesley (1988).
[28] O.V. Lounasma, Experimental Principles and Methods Below 1 K, Academic Press (1974).
[29] Anotec Separations, 226 East 54th St., New York, NY 10022.
[30] Emerson & Cummings, 869 Washington St., Canton, MA 0201.
[31] Available from TRI Research, 2303 Wycliff St., #2W, St. Paul, MN 55114. (GE is a registered trademark of General Electric Co.).
[32] L.M. Steele, C.J. Yeager and D. Finotello, Phys. Rev. Lett., 71 (1993) 3673.
[33] C.J. Yeager, L.M. Steele and D. Finotello, Phys. Rev., B49 (1994) 9782.
[34] D. Finotello, K.A. Gillis, A. Wong and M.H.W. Chan, Phys. Rev. Lett., 61 (1988) 1954.
[35] S. Qian, G.S. Iannacchione and D. Finotello, Phys. Rev., E53 (1996) R4291.
[36] G.S. Iannacchione and D. Finotello, Phys. Rev. Lett., 69 (1992) 2094; Phys. Rev. E 50, 4780 (1994).